N63-12553

code-1
554200
42p
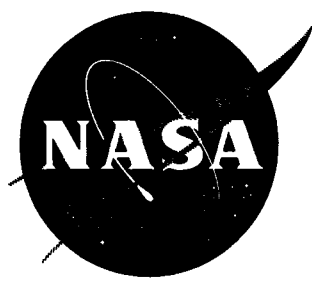
TECHNICAL MEMORANDUM

X - 65

STATIC LONGITUDINAL AERODYNAMIC CHARACTERISTICS OF

SEVERAL WING AND BLUNT-BODY SHAPES APPLICABLE

FOR USE AS REENTRY CONFIGURATIONS AT A

MACH NUMBER OF 6.8 AND ANGLES OF

ATTACK UP TO 90°

By Jim A. Penland and William O. Armstrong

Langley Research Center
Langley Field, Va.

OTS PRICE

XEROX $

MICROFILM $

NATIONAL AERONAUTICS AND SPACE ADMINISTRATION

WASHINGTON   October 1959

CONFIDENTIAL

NATIONAL AERONAUTICS AND SPACE ADMINISTRATION

TECHNICAL MEMORANDUM X-65

STATIC LONGITUDINAL AERODYNAMIC CHARACTERISTICS OF

SEVERAL WING AND BLUNT-BODY SHAPES APPLICABLE

FOR USE AS REENTRY CONFIGURATIONS AT A

MACH NUMBER OF 6.8 AND ANGLES OF

ATTACK UP TO 90°*

By Jim A. Penland and William O. Armstrong

SUMMARY

The static longitudinal stability and trim characteristics of several basic wing and blunt-body reentry shapes are presented along with some estimates made by the modified Newtonian and shock-expansion theories. Experimental data were obtained from an investigation made in the Langley 11-inch hypersonic tunnel at a Mach number of 6.8 through an angle-of-attack range up to 90°. Results of this investigation show that wing plan form has no noticeable effect on the lift-drag ratio of thin flat wings at very high angles of attack and that the maximum lift coefficient of these wings is affected by plan form, but there are indications that no appreciable change in maximum lift coefficient should be expected with increasing Mach number in the high hypersonic speed range. It was also found that the blunt-body shapes tested have static aerodynamic characteristics suitable for use as reentry vehicles and are capable of being trimmed at lift-drag ratios sufficiently high to permit limited control over range and reentry deceleration.

INTRODUCTION

Current interest in manned vehicles with orbital capability has created an intense need for aerodynamic data on configurations applicable for use in reentry designs. Such problems as reentry heating, deceleration, and range control are all dependent upon the aerodynamic

---

*Title, Unclassified.

CONFIDENTIAL

characteristics of the reentry vehicle. Considerable effort has been devoted to the problem of the reentry of a manned vehicle which has the capability of limited control over range and deceleration during the reentry trajectory. Analysis of a capsule or blunt-body type of reentry vehicle is presented in reference 1. Additional analysis of the reentry characteristics of a vehicle utilizing some lift is also presented in reference 2, and a discussion of some methods of controlling the trajectories of high-drag—low-lift vehicles entering the earth's atmosphere is presented in reference 3. Reference 1 shows that when some lift is introduced as well as drag, considerable control over both reentry deceleration and range can be obtained by variations in the lift-drag ratio of the configuration. A knowledge of the longitudinal stability characteristics and trim capability of the vehicle are, therefore, essential for development of a workable design. Results of a preliminary investigation of these characteristics are presented in reference 4.

The purpose of this paper is to present more detailed results of an experimental investigation along with theoretical calculations of the longitudinal stability characteristics of configurations which depend on drag primarily during reentry. These configurations include some basic wing plan forms, a high-drag manned-satellite reentry model with drag-type flaps and various forward faces, and a medium-drag reentry shape with lifting-type flap controls. This investigation was carried out at a Mach number of 6.8 in the Langley 11-inch hypersonic tunnel. Forces and moments were measured by means of strain-gage force balances through an angle-of-attack range up to 90°.

SYMBOLS

C_L lift coefficient, $\dfrac{F_L + F_{A,bp} \sin \alpha}{qS}$

C_D drag coefficient, $\dfrac{F_D + F_{A,bp} \cos \alpha}{qS}$

L/D lift-drag ratio, C_L/C_D

C_m pitching-moment coefficient, $\dfrac{M_Y}{qS\bar{c}}$

$C_{L_\alpha} = \dfrac{\partial C_L}{\partial \alpha}$

ΔC_D change in drag coefficient

$$C_{m_i} = \frac{\partial C_m}{\partial i_f}$$

$$C_{m_\alpha} = \frac{\partial C_m}{\partial \alpha}$$

$$C_p = \frac{p - p_\infty}{q}$$

$$F_L = F_N \cos \alpha - F_A \sin \alpha$$

$$F_D = F_N \sin \alpha + F_A \cos \alpha$$

F_N	normal force
F_A	axial force
M_Y	pitching moment
$F_{A,bp}$	base-pressure correction
q	free-stream dynamic pressure
S	reference area (wing plan-form area, maximum body cross-sectional area, or frontal area as noted)
$\bar{c}$	diameter of body or wing
l	length of body
M	free-stream Mach number
r	radius
α	angle of attack, deg
α_{trim}	angle of attack for $C_m = 0$, deg
γ	ratio of specific heats, 1.4 for air
i_f	flap deflection (zero when flap is parallel to model center line), deg
p_∞	free-stream static pressure

p   local static pressure

Subscript:

max   maximum

CONFIGURATIONS TESTED

The models used for the present tests consisted of seven basic models with three of the seven having flaps which were deflected various amounts to affect trim. These models are shown in the photographs in figure 1, and the details and basic dimensions are presented in figure 2. The circular, square, and 30° delta wings were flat plates 0.031 inch thick with rounded leading edges. Tests were also made on the circular wing with one circumferential flap attached as shown in figure 2(a) which was deflected 45° and 90°. The remaining four reentry bodies shown in figure 2 consisted of a frustrum of a 15° half-angle cone with a sphere replacing the vertex which has a radius equal to one-third of the maximum body diameter. A common body was used with interchangeable forward faces to encompass the convex-faced, small flat-faced, and enlarged flat-faced reentry bodies (figs. 2(d), 2(e), and 2(f), respectively). Flaps were installed on the outermost edge of the forward face of the convex-faced reentry body. Tests were made by using both three flaps and one flap as indicated in figure 2(d). The area of each flap used on the convex-faced reentry body was about 4.5 percent of the circular frontal area which was selected as the reference area for this model.

The blunt conical reentry body (fig. 2(g)) utilized the same body shape as the other reentry configurations except that it was oriented such that the small spherical end faced the flow and trailing-edge flaps were installed. The total plan-form area of these flaps was about 18 percent of the reference area of this configuration, but only about 9 percent was considered effective because of blanketing by the body.

APPARATUS AND TEST PROCEDURES

The tests were conducted in the Langley 11-inch hypersonic tunnel at an average Mach number of 6.8, a stagnation pressure of 15 atmospheres absolute, and an average stagnation temperature of 675° F to avoid liquefaction. This tunnel normally operates at a Mach number of 6.86, but at the reduced stagnation pressure of these tests the Mach number was 6.8. The Reynolds number based on body length was 260,000. The absolute humidity was kept to less than 1.9×10^{-5} pounds of water

per pound of dry air for all tests. Lift and drag forces were obtained
by the use of an external-force balance, and the pitching moment was
measured on a separate one-component balance during separate tests. The
range of angle of attack varied from 0° to 90° for the blunt reentry
shapes and was somewhat less for the wings and the blunt conical reentry
shape. In order to avoid serious sting interference and large base-
pressure corrections, the angle-of-attack range was made in 15° to 25°
steps by presetting the model at an initial angle of attack relative to
the balance and then by rotating the balance and model through the desired
angular step with a movable strut. The true angles of attack were set
optically by use of a point source of light and a small lens-prism assem-
bly mounted on the model sting. The image of the light source was reflec-
ted by the prism and was focused by the lens on a chart. A calibration
was necessary for each model-sting assembly. Model base pressures were
measured during all tests, and the axial-force component was adjusted to
correspond to a base pressure equal to stream static pressure.

ACCURACY OF DATA

The maximum uncertainties in the force and moment coefficients for
the individual test points due to the force balance system are presented
as follows:

Coefficient	Uncertainty
C_L	±0.026
C_D	±0.008
C_m	±0.004

The setting accuracy of the angle of attack was ±0.10°, and the varia-
tion of Mach number was no greater than ±0.01. The stagnation pressure
was measured to an accuracy of ±1.3 in. Hg out of 500 in. Hg abs.

THEORETICAL METHODS

The aerodynamic characteristics of the models at $M = 6.8$ and at
various angles of attack were calculated and the results are presented
along with the experimental data. Various methods were used for differ-
ent models and these methods are discussed in this section.

Flat-Plate Wings

Calculations were made on the flat-plate wings by using the inviscid two-dimensional shock-expansion theory and several modifications of the Newtonian theory. No viscous forces were included in these calculations because it was believed that these effects would be relatively small at the large angles of attack under study. Shock-expansion calculations for these wings were based on free-stream Mach numbers of 6.8 and ∞ and assumed attached flow in all cases.

In order to provide more insight into the angle-of-attack regions beyond that for shock detachment ($\alpha = 43°$ for $M = 6.8$) where the shock-expansion theory is no longer valid, calculations were made by using the Newtonian and modified Newtonian theories. The Newtonian theory (ref. 5) makes use of the relation $C_{p,local} = C_{p,max} \sin^2\alpha$ where α is the angle of attack and $C_{p,max}$ is the stagnation pressure coefficient which from pure momentum considerations is equal to 2; therefore, $C_{p,local} = 2 \sin^2\alpha$. The modified Newtonian theory concept, which was arrived at experimentally in 1954 in reference 6 and given theoretical justification in reference 7, uses the stagnation pressure coefficient from normal-shock theory for $C_{p,max}$. This modification of the Newtonian theory referred to as blunt-nosed modified Newtonian (ref. 8) is given as $C_{p,local} = 1.822 \sin^2\alpha$ for $M = 6.8$ and was used primarily to obtain the integrated values of forces and moments on wings at angles of attack above that for shock detachment. Calculations made by this method will hereinafter be referred to as modified Newtonian $C_{p,max} = 1.822$.

Another theory described by the equation $C_{p,local} = (\gamma + 1)\sin^2\alpha$ which gives improved results on nonblunted configurations at angles of attack below that for shock detachment also takes the form of the Newtonian concept and is called flat-plate modified Newtonian (ref. 8); this theory was suggested by Laitone (ref. 9) in 1947 as a good approximate method for obtaining local pressure coefficient at large free-stream Mach numbers. This relation will be referred to as modified Newtonian $C_{p,max} = \gamma + 1$ throughout the remainder of this paper. This concept is most applicable to wings at angles of attack below that for shock detachment and is used to calculate the wing forces in the low angle-of-attack range.

Another approach using a semiempirical procedure to estimate the forces on winged configurations at angles of attack above shock detachment is presented in reference 10. However, that method is dependent

on an arbitrary fairing between the angle of attack for shock detachment and the maximum normal-force coefficient and is, therefore, not included in this paper.

Blunt Bodies

Theoretical estimates of the force coefficients of the blunt-body shapes studied in this paper were made by summing up the individual forces on the conical, spherical, and flat surfaces by using the modified Newtonian concept $C_{p,max} = 1.822$. The pitching-moment coefficients were obtained by a summation of the individual moments contributed by each body component. The flat body faces were assumed to contribute no pitching moment. Viscous effects were neglected, and the base pressure was assumed to be equal to free-stream static pressure in these calculations.

Flaps

Convex-faced reentry body.- The pitching-moment contribution of the flap on the convex-faced reentry body was calculated at $\alpha = 0^\circ$ for various flap deflections by using the modified Newtonian theory $C_{p,max} = 1.822$. The flap-effectiveness parameter C_{m_i} was determined from a plot of calculated values of C_m against flap deflection.

Blunt conical reentry body.- Calculations of the flap effectiveness on the blunt conical reentry body were made by using the modified Newtonian theory $C_{p,max} = \gamma + 1$. Calculations of the flap effectiveness which were made by using this theory were made by considering the local Mach number on the body in the region of the trim flaps which were located behind a strong detached nose shock. The local Mach number over the body was determined through use of data presented in reference 11 at a free-stream Mach number of 5.8. Data presented in this reference showed the ratio of the local pressure coefficient at various body stations to the stagnation pressure coefficient for a series of spherical-nosed cones of varying semiapex angles. Although no data were shown in reference 11 for the cone angle under consideration, the value of $C_p/C_{p,max}$ was obtained by interpolation of a cross plot of the results presented in reference 11. Comparison of this ratio of $C_p/C_{p,max}$ with data obtained in the Langley 11-inch hypersonic tunnel at $M = 6.8$ on a hemisphere-nosed cylinder (ref. 12) and on a 10° half-angle spherical-nosed cone (unpublished data obtained by Daniel J. McKinzie, Jr., at $M = 6.8$) indicates that the ratio $C_p/C_{p,max}$ was not greatly affected by Mach number in this hypersonic Mach number range. Since the data

presented in reference 11 appeared to agree closely with data at the test Mach number of this study, the value of $C_p/C_{p,max}$ was determined from reference 11 at the body position where the trim flaps were attached. By knowing this pressure ratio, the local Mach number and pressure on the body surface were determined in the region of the trim flaps based on a free-stream Mach number of 6.8. Although a Mach number gradient is known to exist along the span of the flap, this surface condition was considered sufficiently accurate for estimating flap effectiveness. The effective area considered was the exposed area which was 9 percent of the reference area and located outside of a line parallel to and on the body surface; thus, no estimate was included to account for either the expanded flow or separated flow or both over the flap in the shadow region of the body.

Calculations of flap effectiveness by using modified Newtonian theory $C_{p,max} = \gamma + 1$ assumed the local flow conditions described previously. The pressure coefficient of the flap was determined by using the relation $C_p = (\gamma + 1)\sin^2 i_f$ and was corrected to free-stream conditions by the ratio of the local dynamic pressure to the free-stream dynamic pressure.

RESULTS AND DISCUSSION

Wings of Various Plan Forms

A comparison of the lift and drag of three wings having circular, square, and delta plan forms is presented in figure 3 along with flat-plate calculations made by the shock-expansion theory and two modifications of the Newtonian theory. The data for wings at angles of attack up to 42.6° were taken from references 13 and 14. Wings used in references 13 and 14 had a thickness-chord ratio of 0.05 and sharp leading edges in contrast with the wings tested in this investigation which were flat plates with rounded leading edges. The delta wing in reference 14 also had a 26° vertex angle instead of the 30° vertex angle in this paper. The data presented for angles of attack from 44° to 90° were obtained during the present investigation.

A selection of typical schlieren photographs is presented in figure 4 of the three wing plan forms. A study of these photographs shows a variation in the shock geometry with changing wing plan form and indicates the probability of some pressure-relieving effects in the vicinity of the vertex of the delta wing. It may be seen, however, from figure 3 that plan form has little or no effect on the longitudinal force characteristics of these wings at the high-angle-of-attack conditions $(\alpha > 70°)$ although the geometry of the bow shock waves is altered because of model

shape. Variations in the values of C_L and C_D at a given angle of
attack due to plan form may be noted as the angle of attack is reduced
below about 70°. The experimental data indicate that the circular- and
square-plan-form wings have higher lift and drag, respectively, than the
delta wing at these lower angles of attack but that the L/D ratio
remains essentially independent of plan form throughout the angle-of-
attack range. This trend of higher lift and drag for the square-plan-
form wing as compared with that for the delta-plan-form wing is evident
at lower angles of attack as shown by the experimental data from refer-
ences 13 and 14. An explanation of the flow phenomenon that is respon-
sible for this trend is at least twofold. The variation in the lower
angle-of-attack region is primarily caused by the early leading-edge
shock detachment on the delta wing, whereas at an angle of attack near
$C_{L,max}$ the variation in C_L and C_D with changing wing plan form
appears to be related to the variation of wing perimeter with plan-form
area. Experimental data show that as the ratio of perimeter to plan-
form area increases (with the plan form changing from circular to delta),
the value of the forces is reduced in the angle-of-attack range between
45° and 60°; the reduction is probably due to edge losses resulting from
high-pressure flow from the wing lower surface to the wing upper surface.
However, this variation in C_L and C_D with wing plan form is notice-
able only in the medium angle-of-attack region (α = 45° to 60°) and
disappears as α approaches 90°.

A comparison of the predicted lift and drag characteristics obtained
by using several theoretical approaches with those determined experi-
mentally is also presented in figure 3. Calculations made by using the
two-dimensional shock-expansion theory, although with leading-edge and
viscous axial-force contributions neglected, agree well with experimental
data for both the square- and delta-plan-form wings in the angle-of-
attack region below leading-edge shock detachment. Since this theory
does not account for leading-edge shock-detachment effects, it over-
predicts the forces on wing plan forms where the flow has detached from
the leading edge as shown by the 26° delta-wing data. As shown in fig-
ure 3, the modified Newtonian theory $\left(C_{p,max} = 1.822\right)$ agrees well with
experimental data at the higher angles of attack beyond shock detachment.
The Newtonian theory with $C_{p,max} = \gamma + 1$ provides a more effective
means of predicting the forces on slender bodies and wings in the lower
angle-of-attack range and, as shown in figure 3, gives reasonable pre-
dictions of the force coefficients for these wings at angles of attack
below about 45°.

Maximum Lift Coefficient of Wings

A more detailed study of the lift of flat-plate wings is shown in
figure 5. This figure shows curves of lift coefficient calculated by

the shock-expansion theory at the test Mach number of 6.8 and at M = ∞
up to the respective angles of attack for shock detachment. Within the
limited applicable angle-of-attack range of this theory it may be seen
that the lift coefficient is changed about 10 percent at the higher
angles of attack with a large increase in Mach number. Also shown in
this figure are the values of lift coefficient as calculated by the
Newtonian theory where $C_{p,max} = 2.0$ and the modified Newtonian theory
where $C_{p,max} = 1.822$. These curves obtained by the Newtonian method
show that the maximum value of lift coefficient occurs at an angle of
attack of about 55°, and both Newtonian methods underpredict the experi-
mental data in this region although the unmodified Newtonian theory uses
a value of $C_{p,max}$ that is almost 10 percent higher than the stagnation
pressure coefficient for M = ∞.

From a study of these theoretical methods it appears that only small
changes in lift coefficient can be anticipated in the Mach number region
above 6.8 in continuum flow for wings of this type. The measured results
show that the maximum lift coefficient at M = 6.8 is about 0.85 and it
occurs at angles of attack of about 50°. With consideration of the pre-
viously mentioned theoretical study, it may be anticipated that there
will be little change in the experimental maximum lift coefficient with
increasing Mach number. Therefore, the maximum C_L at M = 6.8 may be
considered representative of the value of maximum C_L that might be
expected at higher Mach numbers. This apparent freeze of maximum lift
coefficient with Mach number is similar to that observed for the drag
coefficient (ref. 4).

The pitching moment of the flat-plate circular wing for various
flap deflections is presented in figure 6 for the high angle-of-attack
range. The data presented in this figure show a gradual increase in
the pitching-moment curve with increasing angle of attack up to an angle
of attack of about 65°. As angle of attack was increased beyond that
for complete shock detachment (α = 43° for M = 6.8), the wing operated
in a region behind an increasingly stronger detached shock as evidenced
by the schlieren photographs shown in figure 7. Since this wing is
operating in a region of subsonic flow behind a strong detached shock,
pressure losses would be expected in the vicinity of the wing periphery
with the greatest losses occurring near the downstream edge of the wing.
This results in an increasingly higher pressure with angle of attack
near the wing leading edge; thus, the nose-up pitching moment is increased
as shown by the experimental results in figure 6. As angle of attack was
further increased (α > 65°), the wing face became more nearly alined nor-
mal to flow and the pressure differential over the wing face decreased;
hence, the pitching moment was reduced. At α = 90° the wing was alined
normal to the flow with the result that a symmetrical pressure distribu-
tion and a zero pitching moment occurred as shown by the experimental

results. Deflection of the wing flap did not noticeably alter the basic
trend of the pitching-moment curve but simply added a nose-down incre-
ment which increased with increasing flap deflection. Comparison of the
experimental data with calculations made by using the modified Newtonian
theory $C_{p,max} = 1.822$ shows rather poor agreement since it does not
account for any of the previously discussed variations of pressure over
the windward surface.

<p style="text-align:center">Reentry Bodies</p>

From the study of flat-plate wings through the angle-of-attack
range up to 90° as discussed in figure 3, it can be seen that a drag
coefficient of about 1.7 can be realized from a flat-plate wing normal
to the flow. A circular wing could conceivably be used for a manned-
satellite reentry configuration if a storage volume in the form of an
afterbody is attached in the downstream or shadow region; the result
would be a vehicle similar to that proposed in reference 1. A group
of configurations based on this concept which utilized a common after-
body has been tested and the untrimmed longitudinal stability charac-
teristics are presented in figure 8 through an angle-of-attack range
from 0° to 90°. Experimental data are compared with predictions cal-
culated by use of the modified Newtonian theory $C_{p,max} = 1.822$. The
maximum body cross-sectional area was used as the reference area in
this figure. It is important to note how the angle-of-attack reference
is oriented for presentation of these data on reentry shapes because it
differs by 90° from that used in the presentation of the wing data.
Such an orientation is desirable to satisfy the stability convention
that a stable pitching-moment curve have a negative slope as well as
to orient the configuration in the conventional attitude for reentry.

It is important to note from these data that these blunt bodies
exhibit a negative lift-curve slope in the lower angle-of-attack range,
a characteristic associated with extremely blunt bodies. From a com-
parison of the experimental results with those obtained by using the
modified Newtonian theory for the flat-faced and convex-faced configu-
rations, it can be seen that the predicted values of C_L agree fairly
well with experimental values for both configurations throughout the
angle-of-attack range. It may be seen that the slope of the lift curve
at the lower angles of attack and the maximum lift coefficient which
occurs at an angle of attack of about 35° for all configurations are
considerably affected by changes in face geometry as a result of the
reference area being held constant and of the face area and shape being
changed.

Trends in C_D are fairly well predicted for these shapes by the
modified Newtonian theory $C_{p,max} = 1.822$; however, as expected, the

tendency of this theory to overpredict the drag coefficient for very
blunt bodies as pointed out in reference 4 is evident from figure 8 in
the low angle-of-attack range. Comparison of experimental pitching-
moment data with calculated pitching-moment data shows the Newtonian
theory to be inadequate for predictions of trends of C_m with angle of
attack for very blunt body shapes.

Effects of varying face geometry.- The comparison of the faired
experimental longitudinal stability characteristics of the convex-faced,
small flat-faced, and enlarged flat-faced reentry bodies having a com-
mon reference area based on the maximum cross-sectional area of the
common body is presented in figure 9. It is important to note that for
angles of attack less than 25° alterations in the front-face geometry
had no noticeable effect on the lift-drag ratio even though the drag
coefficient did change substantially. The maximum attainable L/D
ratio, which is negative here because of the negative lift curves of
these blunt bodies, is, however, dependent on the front-face geometry.
The angles of attack at which $(L/D)_{max}$ occurs increase as the body
bluntness increases. This trend is similar to that which may be calcu-
lated for cones and wedges with increasing bluntness. At the high angles
of attack the body receives the full effect of the free-stream flow (see
schlieren photographs in fig. 7) and the front face is least effective.
The drag coefficient is not appreciably affected in the angle-of-attack
range between 60° and 90°. The curves of the L/D ratio show the
effects of the face geometry on the lift force in this angle-of-attack
range; at angles of attack above about 75° the enlarged flat face shows
the most lift because of the pressure field around the body acting on
the extended rim of the face. The smaller flat face shows only the lift
due to the pressure field over the body, whereas the convex-faced body
shows the smallest lift due to the pressures on the curved face which
are in opposition to the body pressure field.

The variation of the pitching moment with angle of attack depends
markedly upon the configuration, particularly in the high angle-of-
attack region. There were no unexpected changes at low angles of attack.
All models are statically stable up to angles of attack of about 20°.
The enlarged flat-faced model shows the largest value of C_{m_α} at low
angles of attack because of the extended frontal rim and increased moment
arm over which the pressure forces are acting. As angle of attack is
further increased, all three configurations become unstable (posi-
tive C_{m_α}); the angle of attack at which this unstable tendency begins
depends upon the face geometry. The enlarged flat-faced reentry body
maintains its stability to a higher angle of attack than does the small
flat-faced body. This is due to the reduced pressures over the forward
portion of the afterbody in the expansion region of the face forward of
the point of reattachment of the flow. (See the schlieren photograph of

this model at $\alpha = 45^{\circ}$ in fig. 7.) The convex-faced body remains stable
to a higher angle of attack than either of the flat-faced bodies because
of the relieving effect of the pressures on the downstream side and the
higher pressure region on the forward portion of the curved face, which
contribute stabilizing pitching moments. At the very high angles of
attack (near 90°) the convex-faced body shows little change in pitching
moment with angle of attack. The downward or negative lift produced by
the forward portion of the curved face and the drag on the afterbody
both produce negative pitching moments that are not appreciably affected
by changes in angle of attack in this angle-of-attack range. The small
flat-faced body has little or no pressure on the face to produce pitching
moments; and the pressures on the afterbody, therefore, give a negative
slope to the pitching-moment curve at the higher angles of attack. The
enlarged flat-faced reentry body, like the smaller flat-faced body, has
little or no pitching moment producing pressures on the front face at
high angles of attack. However, in addition to the negative pitching
moment producing pressure forces on the body, there is a large positive
pitching moment produced by the body pressure field acting on the bottom
forward side of the extended rim of the face, which produces a positive
pitching moment and a positive slope to the curve.

Effects of afterbody addition.- A comparison has been made in fig-
ure 10 of the longitudinal stability characteristics of the small flat-
faced reentry body, the enlarged flat-faced reentry body, and the flat
circular wing. In this comparison, the data from the circular wing are
presented with the zero-angle-of-attack axis perpendicular to the wing
surface. The frontal area of each model was taken as the reference area
in order to compare the effects of the afterbody addition. This differs
from the results presented in figures 8 and 9 which referenced the maxi-
mum body cross-sectional area.

Figure 10 shows that the pitching-moment coefficient and, hence,
$C_{m_{\alpha}}$ are not affected by the addition of an afterbody at angles of attack
near 0°. This conclusion is supported by data presented in reference 15.
Examination of schlieren photographs in figure 7 of these various flat-
faced configurations shows that the afterbody additions have little effect
on the shock geometry at $\alpha = 0^{\circ}$, a fact which further indicates that the
afterbody has a negligible influence on the flow characteristics around
the forward face. As the angle of attack was increased up to about 25°,
the effect of afterbody addition tends to increase the stabilizing
pitching moment as shown in figure 10. As previously discussed, the wing
alone loses its stabilizing pitching moment as angle of attack is increased
above $\alpha = 25^{\circ}$ because of the changing pressure field behind the detached
shock. Addition of an afterbody tends to offset this loss in pitching
moment because of the restoring moment contribution of the afterbody sec-
tion. The configuration with the smaller afterbody has the least unstable
slope in the angle-of-attack region between $\alpha = 25^{\circ}$ and 40° and is

probably due to a combination of the lower pressure in the expansion
region behind the body face and the higher afterbody pressure accom-
panying the impingement of the oblique shock on the afterbody of the
configuration. (See the schlieren photographs of this model at $\alpha = 45^\circ$
and 60° in fig. 7.) This lower pressure region forward of the body
moment center and the higher afterbody pressure behind the moment center
produce a greater restoring pitching moment on the configuration with
the smaller afterbody as shown in figure 10. As previously noted,
although the configuration with the small afterbody remains unstable at
all angles of attack above about 30° (fig. 10), the model with the large
afterbody again has a stable region at angles of attack above 70°.

At angles of attack up to about 40°, no significant changes in C_D
are evident; however, the curves of L/D show that the values of the
lift coefficient are reduced with increasing afterbody. In the high
angle-of-attack range the drag coefficient is increased and the L/D
ratio is reduced as the size of the afterbody is increased as expected.

Trimmed characteristics of convex-faced reentry body.- In order to
trim at angles of attack, a flap was installed on the convex-faced
reentry body; the results of the tests are presented in figure 11 for
flap deflections of -45°, -90°, and -140° through an angle-of-attack
range from 0° to 90°. Except for pitching moment these data show trends
similar to the untrimmed characteristics presented in figure 8. Schlie-
ren photographs of the convex reentry body at different angles of attack
with various flap deflections are shown in figure 12.

In order to compare the pitching-moment characteristics of this
configuration for the various flap deflections, the faired experimental
variation of C_m with angle of attack is presented in figure 13 for the
different flap settings for α from 0° to 45°. The pitching-moment
characteristics of the circular wing alone using the same trim flap as
the reentry body are also presented in this figure. It should be noted
that the data for the circular wing are shown in figure 13(b) with the
axis system rotated 90° and the location of the center of gravity altered
from that in the presentation of the basic data in figure 6. Although
it has been shown in figure 9 that face geometry has considerable effect
on the pitching moment of this type of configuration at angles of attack
above 20°, a comparison of the pitching-moment characteristics of the
wing alone with those of the convex-faced reentry body in figure 13(a)
shows that the basic trim characteristics of the two are similar at
$\alpha = 20^\circ$. In the low angle-of-attack range $(\alpha < 20^\circ)$, the flow around
the body face should also be similar and this is indeed the case as may
be seen in the schlieren photographs in figure 12.

It can be seen from figure 13 that both configurations are stable
through the low angle-of-attack range regardless of flap deflection and

that the effectiveness of the flap in producing pitch increases as flap
deflection is increased. It can also be seen that the stabilizing
moment contribution of the afterbody is not noticeably altered with
changing flap setting. It is interesting to note that the incremental
pitching moment for a given flap deflection remains essentially constant
over the angle-of-attack range presented. Thus, the moment contribution
of the flap is almost independent of angle of attack.

A comparison of the effect of trim flap deflections on the longi-
tudinal trim characteristics of the convex-faced reentry configuration
is shown in figure 14. Data presented in this figure for $i_f = 0^O$
used the test results obtained from the configuration with no flaps.
Although the addition of a flap set at a deflection of 0° might cause
a slight alteration in the aerodynamic characteristics of the model,
it was believed that for the comparative purposes of this figure the
results shown would not have been noticeably changed by using a model
with a 0° flap deflection instead of no flaps. From figure 14 it may
be seen that this configuration can be trimmed at angles of attack as
high as 22° with a flap deflection of -140°. It can also be seen that
it is possible to attain a trimmed L/D of approximately -0.30 with
the maximum flap deflection of the test. By extrapolation of the data
presented in reference 1 it can be seen that, for the initial conditions
described in this reference, this variation in trimmed L/D with varying
flap deflections allows a control over touchdown of about 400 miles.
This indicates that reasonable control can be maintained over a vehicle
of this type by using this flap arrangement if a flap size of about
5 percent of the reference area is used.

The change in pitching moment due to flap deflection at zero angle
of attack and the flap-effectiveness parameter C_{m_i} are presented in

figure 14 along with calculations made by the modified Newtonian theory
$C_{p,max} = 1.822$ by the procedure described in the section of this paper
entitled "Theoretical Methods." It can be seen that the ability of the
flap to produce pitching moment increases with the angle of flap deflec-
tion and that the calculations follow this trend up to a flap deflection
of about -90° or when the flap is perpendicular to the flow. A further
increase in flap deflection to -140° produces a further increase in the
experimental pitching moment, but the calculations fail to predict this
trend because the theory does not take into account the local flow con-
ditions on the face of the model. A calculated value of flap-
effectiveness parameter C_{m_i} is also presented in figure 14 along

with faired experimental results for the four flap deflections of the
test. Although some differences are shown between experimental and cal-
culated values of C_{m_i}, particularly for flap deflections greater than

-90°, insufficient experimental data were available for making a careful

comparison between theory and experiment. Experimental values of the lift-curve slope C_{L_α} and incremental drag ΔC_D are also shown in figure 14. No significant changes were noted in C_{L_α} with varying flap deflections; however, as expected, incremental drag increased as flap deflection was increased.

Effect of the addition of lateral flaps.- The need of high drag and the usefulness of some lift in accomplishing reentry are well known. By use of additional flaps, both the drag and the lift can be altered through a limited range. Two lateral flaps have been installed normal to the flow on the convex-faced reentry body, and the basic results of longitudinal-stability tests are presented in figure 15 for three trim flap deflections by using the maximum body cross-sectional area as a reference. Schlieren photographs of the flow around this body with lateral flaps are shown in figure 12, and it may be seen that these flaps cause visible disturbances although they are located behind a detached shock. In order to compare the effects of the addition of these lateral flaps, a representative plot of the longitudinal stability characteristics with and without lateral flaps for a flap deflection of -90° is shown in figure 16. It may be seen that the addition of the lateral flaps had a negligible effect on the pitching-moment character-istics throughout the angle-of-attack range and that the angle of attack for trim was not altered. The addition of approximately 9 percent fron-tal area in the form of the two lateral flaps resulted in an appreciable increase in the drag through the angle-of-attack range with about a 6-percent increase in drag coefficient at $\alpha = 0°$. This increase in drag should not be expected to be directly proportional to the increase in frontal area because of the relieving effect of the flow about the edges of the flaps.

A study of the curve of lift-drag ratio indicated that there was a substantial increase in the lift due to the lateral flaps which, with the increased drag, resulted in there being no appreciable change in the trimmed lift-drag ratio. There was, however, a slight increase in the maximum value of L/D. The longitudinal stability characteristics of the trim flap deflections of -45° and -140° exhibit trends similar to those shown in figure 16.

Blunt conical-nosed reentry body.- Thus far this paper has dealt with wings and bodies at high angles of attack and high drag coefficients have been emphasized. The next reentry configuration to be discussed which is a blunt conical-nosed reentry body has medium drag, exhibits normal lift characteristics, and makes use of trailing-edge flaps as trimming devices. The longitudinal stability characteristics of this configuration are presented in figure 17 for the body alone with no flaps

and with flap deflections of 0°, -20°, and -40° along with calculations made with the modified Newtonian theory $C_{p,max}$ = 1.822 for the body alone.

This body is statically stable about the 50-percent body-length station either with or without flaps, and it exhibits a positive lift-curve slope. The drag remains nearly constant for the first 10° of angle of attack and then increases rapidly as the conical afterbody becomes effective.

A comparison of the lift coefficient and the pitching-moment coefficient calculated by using the modified Newtonian theory $C_{p,max}$ = 1.822 with the experimental data shows reasonable agreement, but the theory underpredicts the drag coefficient. This underprediction of drag is consistent with other results in reference 4 which show that the drag is underestimated on all but the bluntest of bodies such as spheres and cones with a very high vertex angle. It is of interest to note that the calculations show the same small drag changes with angles of attack up to 10° as those measured experimentally.

Schlieren photographs of the flow around this body with and without flap deflections at angles of attack of 0° and 15° are shown in figure 18. The disturbance due to the flaps is evident particularly at i_f = -20° and -40°; this result indicates that sufficient acceleration of the local flow has taken place, although located behind the detached nose shock, to result in a local velocity greater than sonic speed.

Figure 19 shows the effect of flap deflection on the static longitudinal stability characteristics of the configuration. It can be seen from this figure that this configuration can be trimmed at angles of attack up to about 11° with a -40° flap deflection with a value of trimmed L/D of about 0.1. Comparison of the experimental values of $\left(C_m\right)_{\alpha=0}$ with those calculated by using the modified Newtonian theory $C_{p,max} = \gamma + 1$ gives good agreement throughout the flap-deflection range of the test.

It should be noted that there is a relatively small increase in the flap-effectiveness parameter C_{m_i} during the first 20° of flap deflection, but it increases more rapidly as flap deflection is increased beyond this point. The slope of the lift curve remains essentially unchanged with flap deflections, and the incremental drag ΔC_D increases with increasing flap deflections as expected.

CONCLUDING REMARKS

An investigation to determine the static longitudinal stability
and trim characteristics of several basic wing and blunt-body reentry
shapes has been conducted in the Langley 11-inch hypersonic tunnel at
a Mach number of 6.8. Results of the study of thin flat-plate wings
show that wing plan form has a noticeable effect on maximum lift but
shows no appreciable effect on the lift and drag characteristics at angles
of attack α above 70°. The lift-drag ratio L/D was relatively inde-
pendent of plan form throughout the entire angle-of-attack range. A
theoretical study of the lift of these wing configurations in the high
hypersonic speed range indicated that the lift coefficient does not
change appreciably with increasing Mach number and that the experimental
maximum lift coefficients of about 0.85 for a circular wing and 0.75 for
a 30° delta wing obtained at a Mach number of 6.8 are representative of
those that might be expected at higher Mach numbers.

The results of the study of blunt reentry shapes show that con-
siderable variation of drag coefficient of these blunt reentry shapes
can be made in the low angle-of-attack range, that is, when the flow
is nearly perpendicular to the forward face by an alteration of the
face geometry or by the addition of lateral flaps with no appreciable
change in the lift-drag ratio. Experimental data show that with a
practical center-of-gravity location, these blunt bodies have stable
static longitudinal stability characteristics through the low angle-of-
attack range ($\alpha < 25°$) and that a value of trimmed L/D as high as
about 0.30 can be obtained through use of the simple fins or flaps used
in this investigation.

Comparison of experimental results with calculated results using
the Newtonian concept indicates that in the hypersonic speed range the
use of the modified Newtonian relationship $C_p = C_{p,max} \sin^2\alpha$ where
C_p is the pressure coefficient and $C_{p,max}$ is the stagnation pressure
coefficient provides a useful means for predicting forces on blunt-body
shapes and wings at angles of attack near 90°. However, another modi-
fied form of the Newtonian theory $C_p = (\gamma + 1)\sin^2\alpha$ where γ is the
ratio of specific heats is more effective for predicting forces on wings
or flaps at angles of attack below those for shock detachment.

Langley Research Center,
     National Aeronautics and Space Administration,
          Langley Field, Va., June 22, 1959.

REFERENCES

1. Faget, Maxime A., Garland, Benjamine J., and Buglia, James J.: Preliminary Studies of Manned Satellites - Wingless Configuration: Nonlifting. NACA RM L58E07a, 1958.

2. Eggers, Alfred J., Jr., and Wong, Thomas J.: Re-Entry and Recovery of Near-Earth Satellites, With Particular Attention to a Manned Vehicle. NASA MEMO 10-2-58A, 1958.

3. Eggleston, John M., and Young, John W.: Trajectory Control for Vehicles Entering the Earth's Atmosphere at Small Flight-Path Angles. NASA MEMO 1-19-59L, 1959.

4. Penland, Jim A., and Armstrong, William O.: Preliminary Aerodynamic Data Pertinent to Manned Satellite Reentry Configurations. NACA RM L58E13a, 1958.

5. Grimminger, G., Williams, E. P., and Young, G. B. W.: Lift on Inclined Bodies of Revolution in Hypersonic Flow. Jour. Aero. Sci., vol. 17, no. 11, Nov. 1950, pp. 675-690.

6. Penland, Jim A.: Aerodynamic Characteristics of a Circular Cylinder at Mach Number 6.86 and Angles of Attack Up to 90°. NACA TN 3861, 1957. (Supersedes NACA RM L54A14, 1954.)

7. Lees, Lester: Recent Developments in Hypersonic Flow. Jet Propulsion, vol. 27, no. 11, Nov. 1957, pp. 1162-1178.

8. Love, Eugene S., Henderson, Arthur, Jr., and Bertram, Mitchel H.: Some Aspects of Air-Helium Simulation and Hypersonic Approximations. NASA TN D-49, 1959.

9. Laitone, Edmund V.: Exact and Approximate Solutions of Two-Dimensional Oblique Shock Flow. Jour. Aero. Sci., vol. 14, no. 1, Jan. 1947, pp. 25-41.

10. Dugan, Duane W.: Estimation of Static Longitudinal Stability of Aircraft Configurations at High Mach Numbers and at Angles of Attack Between 0° and ±180°. NASA MEMO 1-17-59A, 1959.

11. Machell, Reginald M., and O'Bryant, William T.: An Experimental Investigation of the Flow Over Blunt-Nosed Cones at a Mach Number of 5.8. GALCIT Memo. No. 32 (Contract No. DA-04-495-Ord-19), June 15, 1956.

CONFIDENTIAL

12. Crawford, Davis H., and McCauley, William D.: Investigation of the Laminar Aerodynamic Heat-Transfer Characteristics of a Hemisphere-Cylinder in the Langley 11-Inch Hypersonic Tunnel at a Mach Number of 6.8. NACA Rep. 1323, 1957. (Supersedes NACA TN 3706.)

13. McLellan, Charles H., Bertram, Mitchel H., and Moore, John A.: An Investigation of Four Wings of Square Plan Form at a Mach Number of 6.9 in the Langley 11-Inch Hypersonic Tunnel. NACA Rep. 1310, 1957. (Supersedes NACA RM L51D17.)

14. Bertram, Mitchel H., and McCauley, William D.: An Investigation of the Aerodynamic Characteristics of Thin Delta Wings With a Symmetrical Double-Wedge Section at a Mach Number of 6.9. NACA RM L55B14, 1955.

15. DeRose, Charles E.: Normal-Force and Pitching-Moment Characteristics for Two Blunt-Nosed Re-Entry Type Bodies From $M = 2.4$ to $M = 4.0$. NASA MEMO 2-4-59A, 1959.
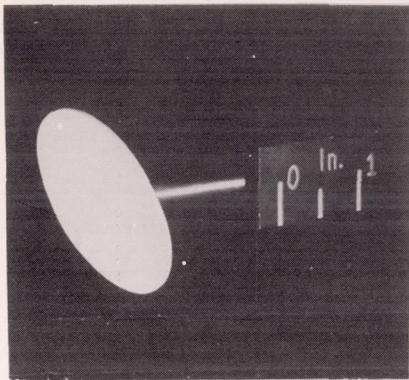
(a) Circular wing.
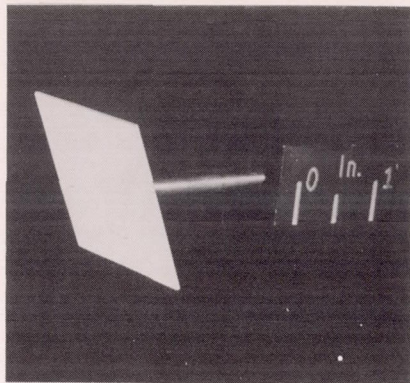
(b) Square wing.
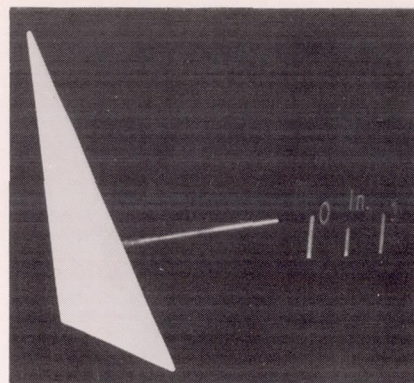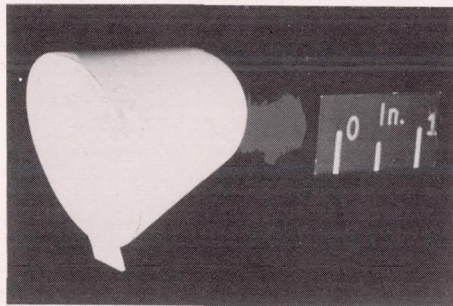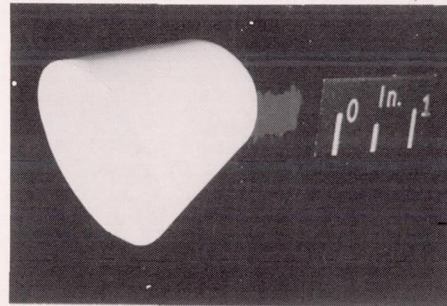
(c) 30° delta wing.

(d) Convex-faced reentry
body.

(e) Small flat-faced
reentry body.
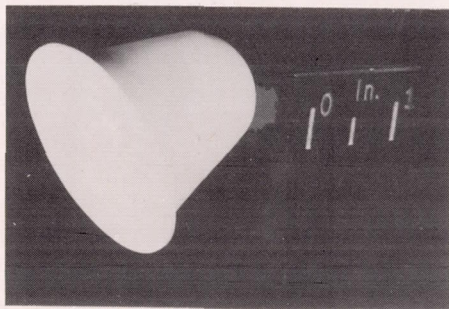
(f) Enlarged flat-faced
reentry body.
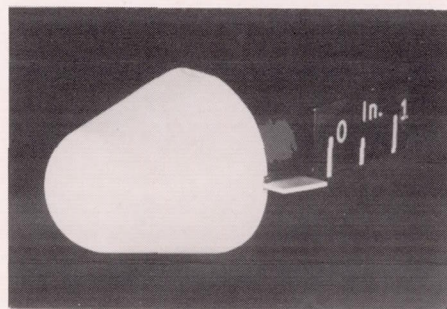
(g) Blunt conical
reentry body.

Figure 1.- Photographs of models tested. L-59-3067
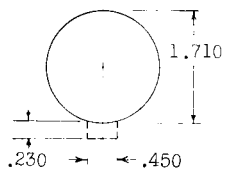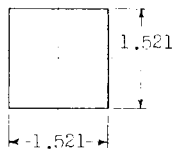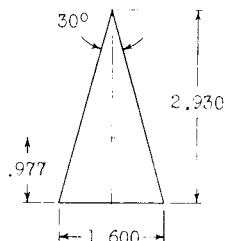
(a) Circular wing.

(b) Square wing.

(c) 30° delta wing.
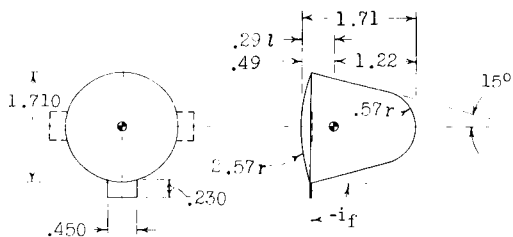
(d) Convex-faced reentry body.
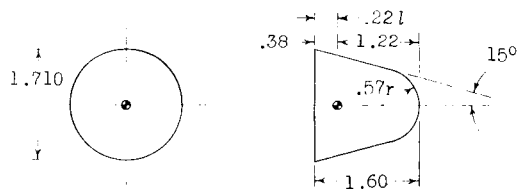
(e) Small flat-faced reentry body.
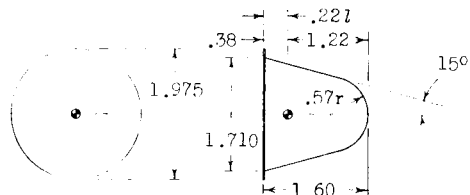
(f) Enlarged flat-faced reentry body.
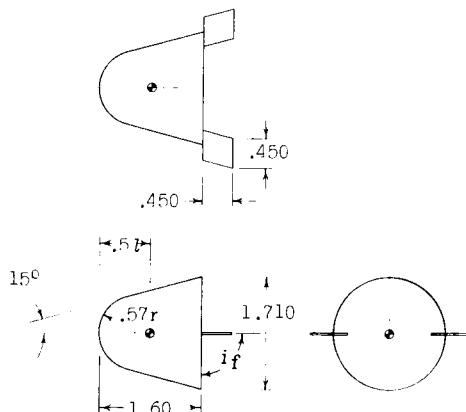
(g) Blunt conical reentry body.

Figure 2.- Details and basic dimensions of models tested. All dimensions are in inches.
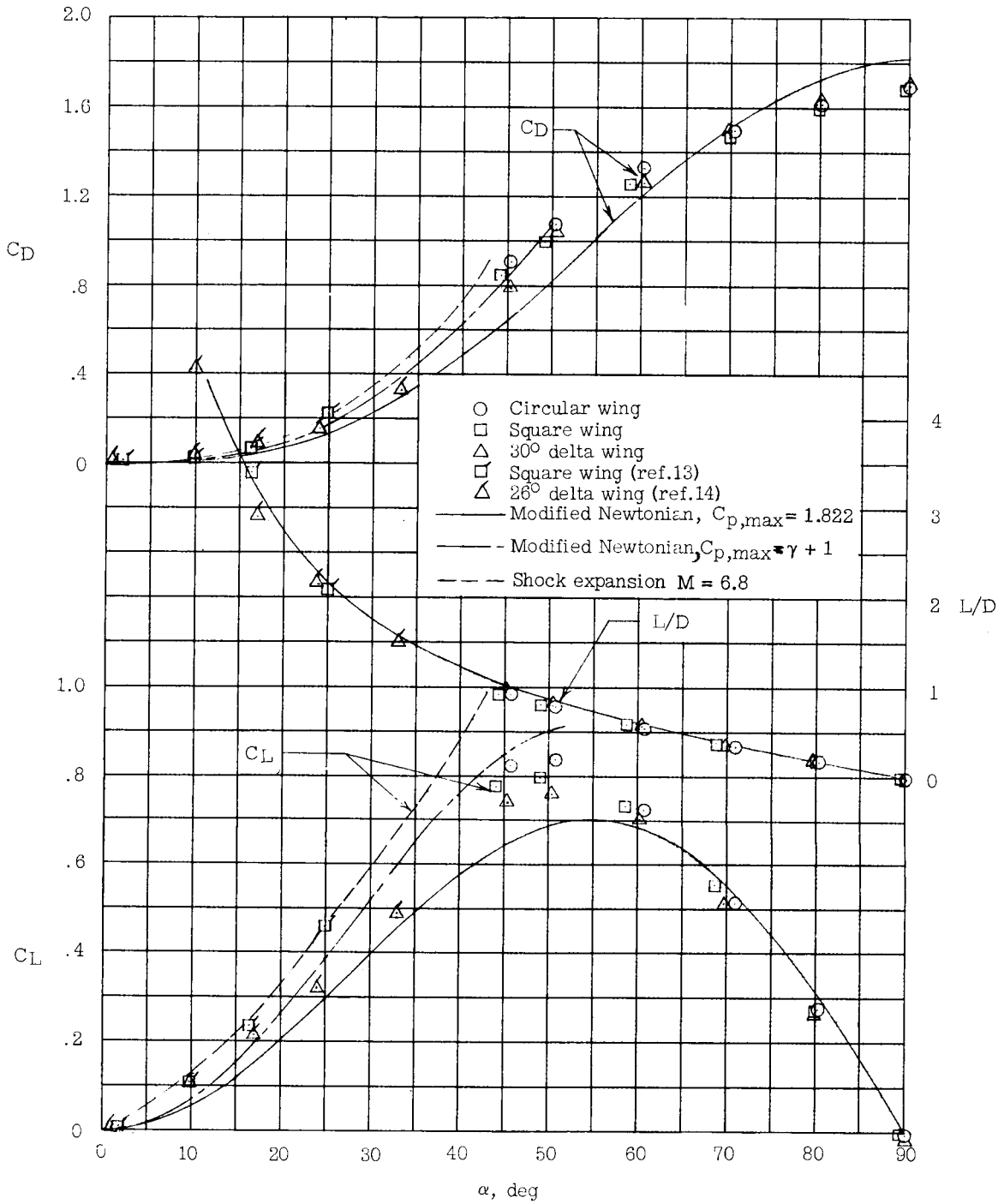
Figure 3.- Comparison of aerodynamic characteristics of circular, square, and 30° delta wings. M = 6.8.

$\alpha = 70^{\circ}$
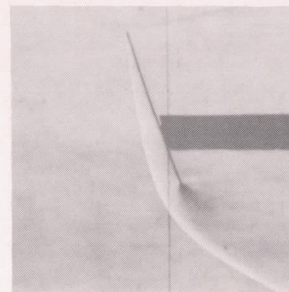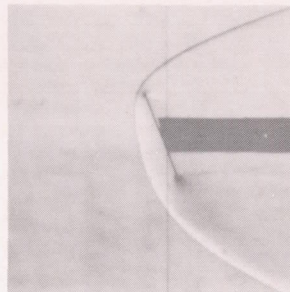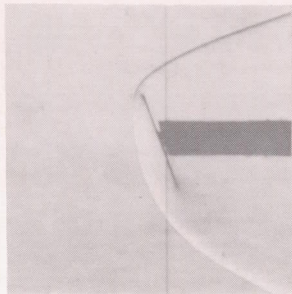
$\alpha = 90^{\circ}$
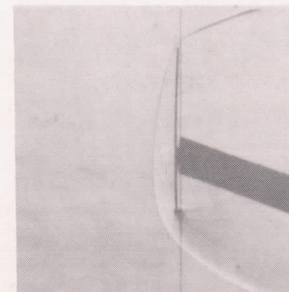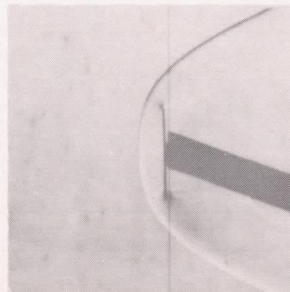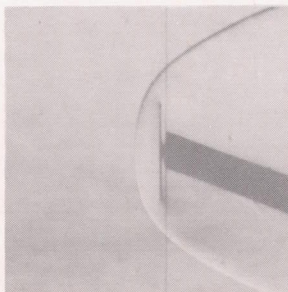
Circular wing   Square wing 30° delta wing

L-59-3068

Figure 4.- Schlieren photographs of flat-plate wings of various plan forms. M = 6.8.
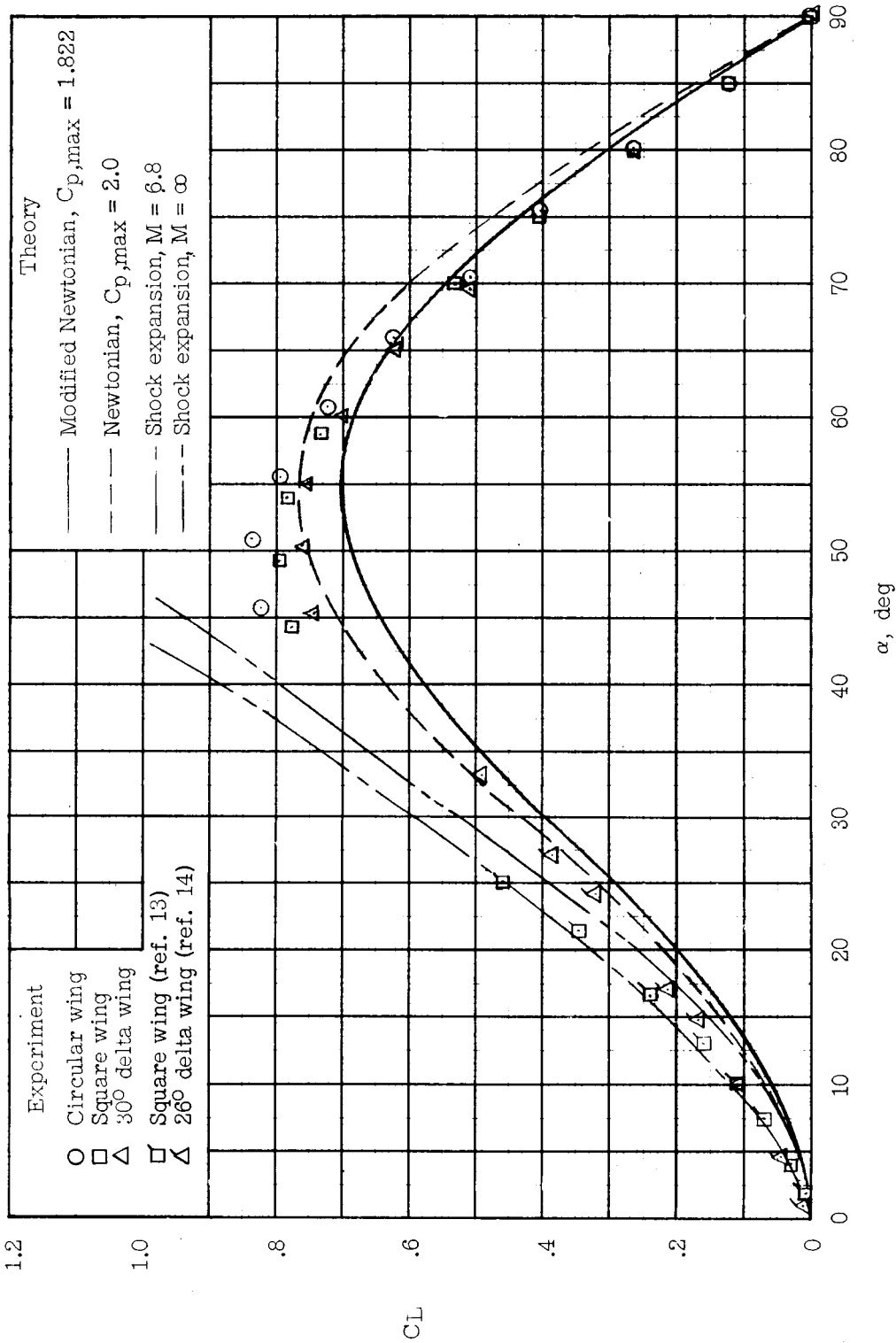
Figure 5.- Comparison of experimental and theoretical lift coefficients of flat-plate wings at angles of attack up to 90°.
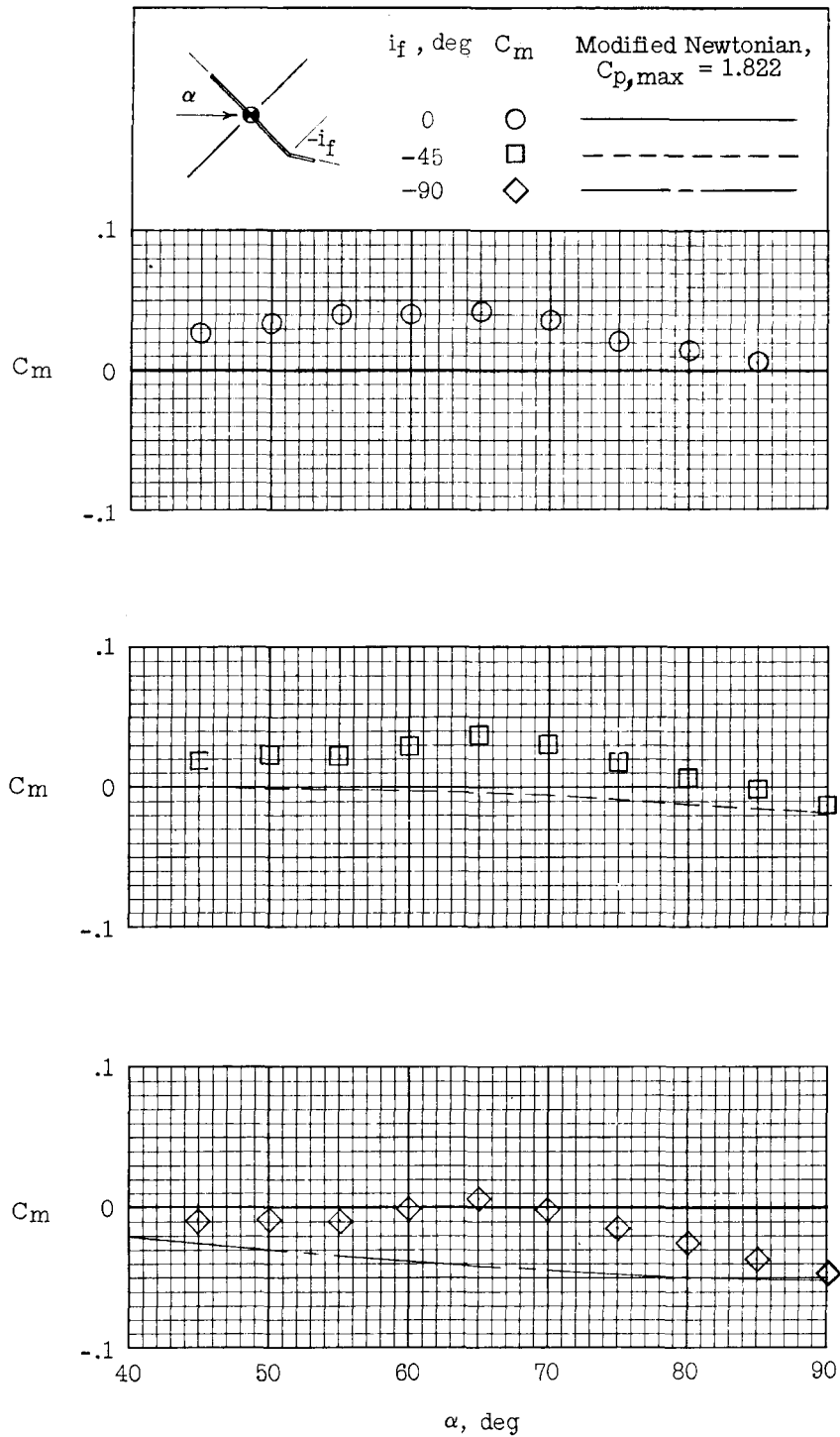
Figure 6.- Pitching moment of circular wing with various flap deflec-
tions. M = 6.86; S, plan-form area excluding flap.

Circular
wing

Small
flat-faced
reentry body

Enlarged
flat-faced
reentry body

Convex-faced
reentry body

$\alpha = 0°$ $\alpha = 25°$ $\alpha = 45°$ $\alpha = 60°$ $\alpha = 90°$
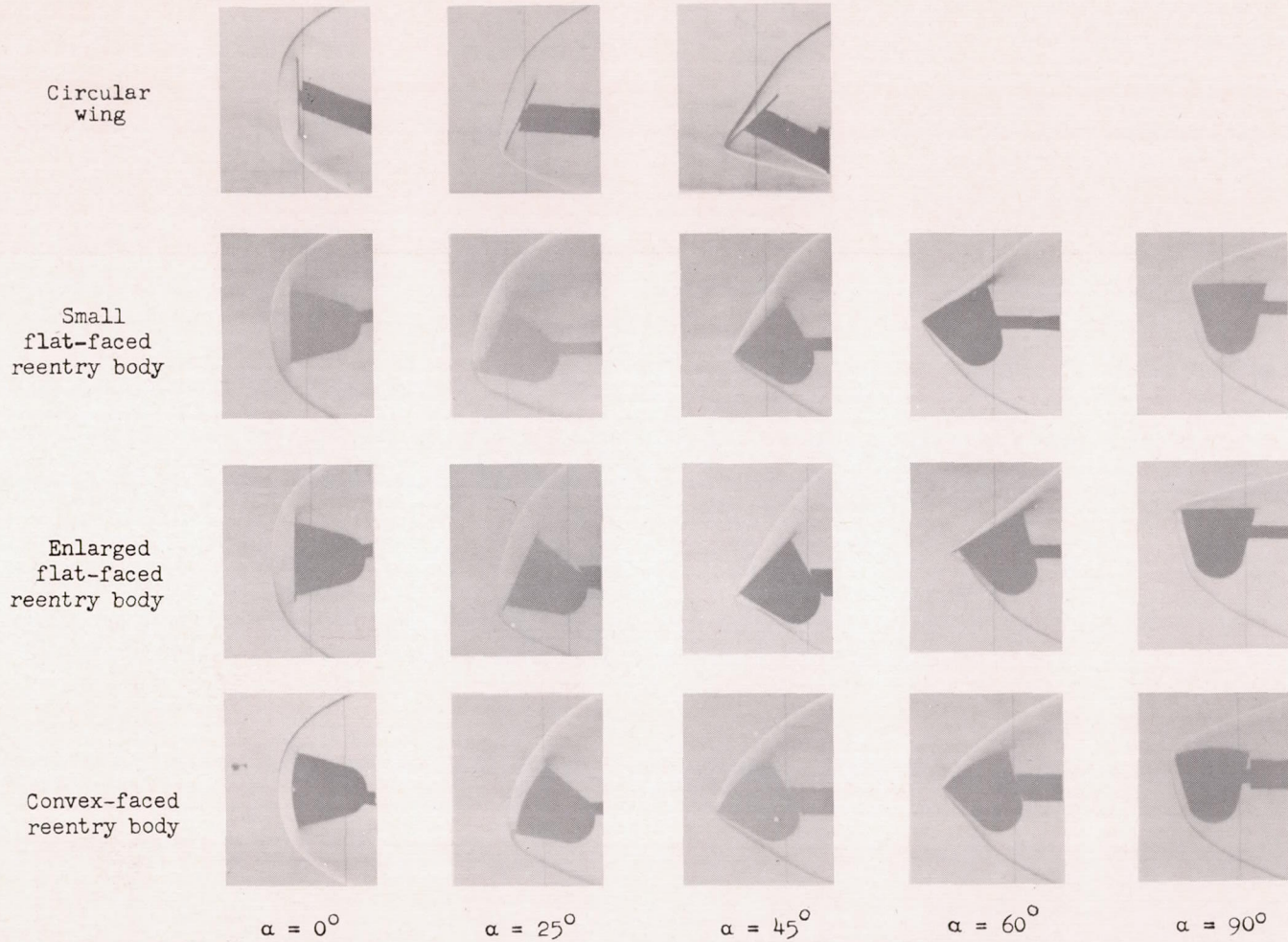
L-59-3069

Figure 7.- Schlieren photographs of several reentry shapes at various angles of attack.
M = 6.8.
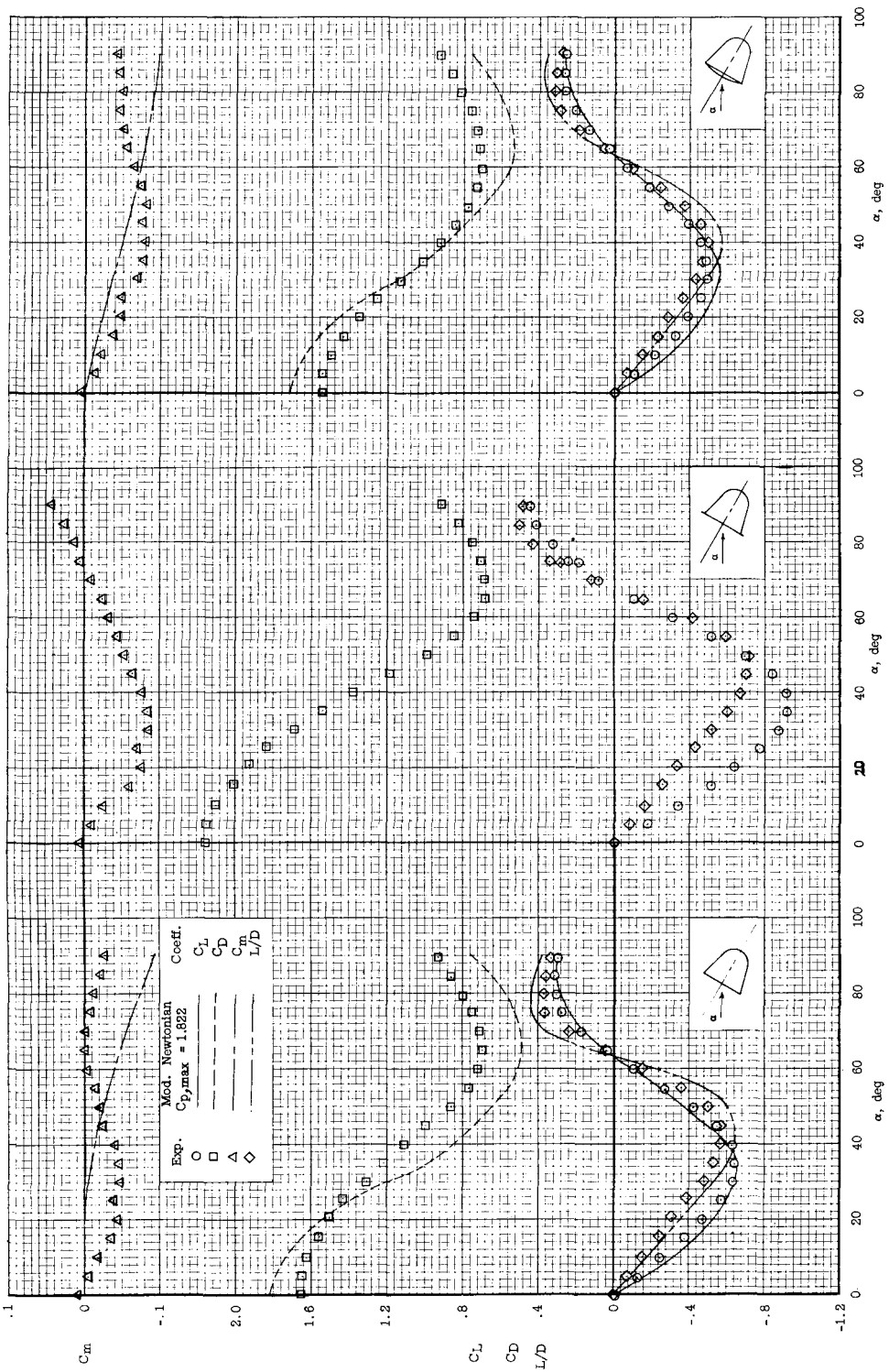
(a) Small flat-faced body.　(b) Enlarged flat-faced body.　(c) Convex-faced body.

Figure 8.- Untrimmed longitudinal stability characteristics of a basic reentry body with differing face geometry. No flaps; M = 6.8; S, maximum body cross-sectional area.
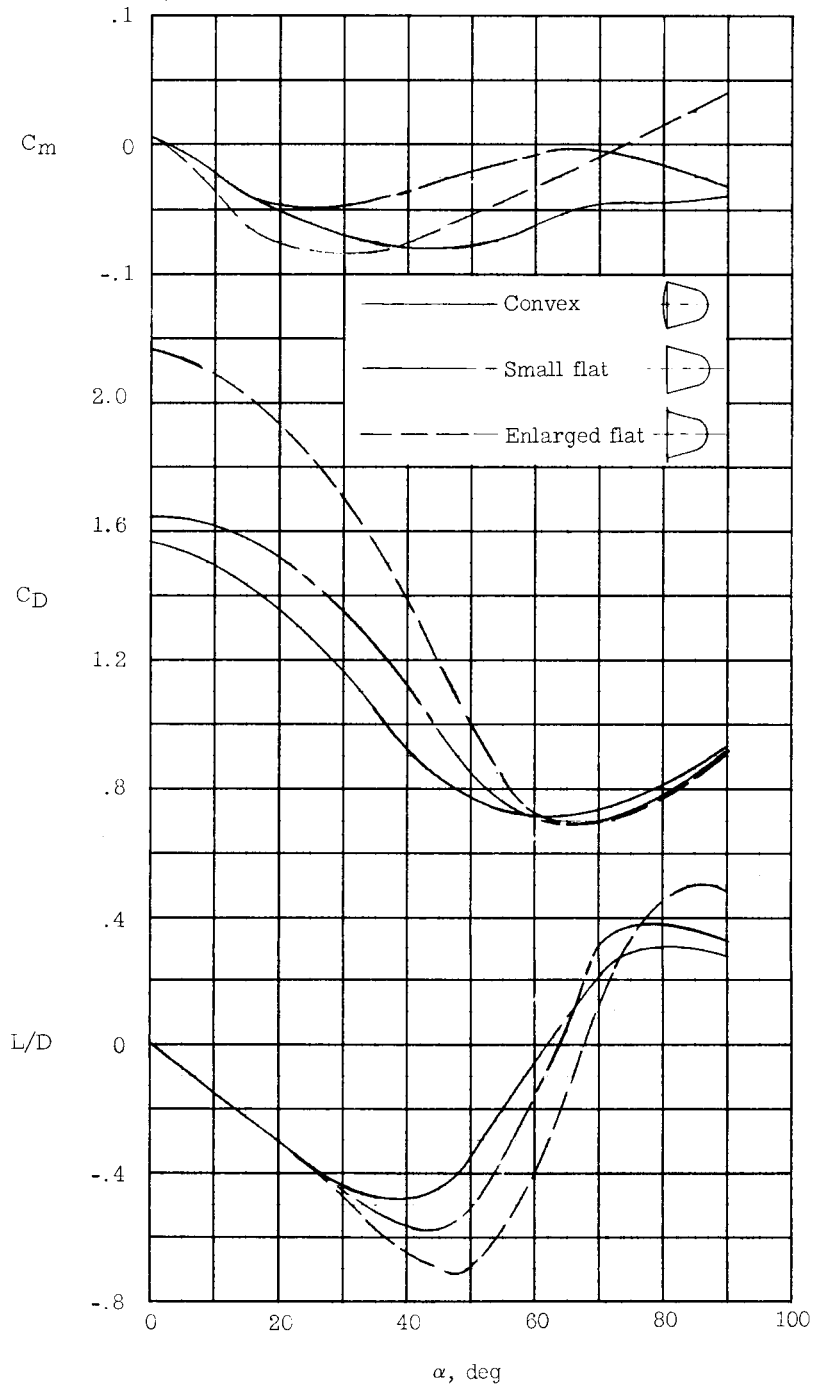
Figure 9.- Comparison of faired experimental longitudinal stability
characteristics of a basic reentry body with differing face geometry.
$M = 6.8$; S, maximum body cross-sectional area.
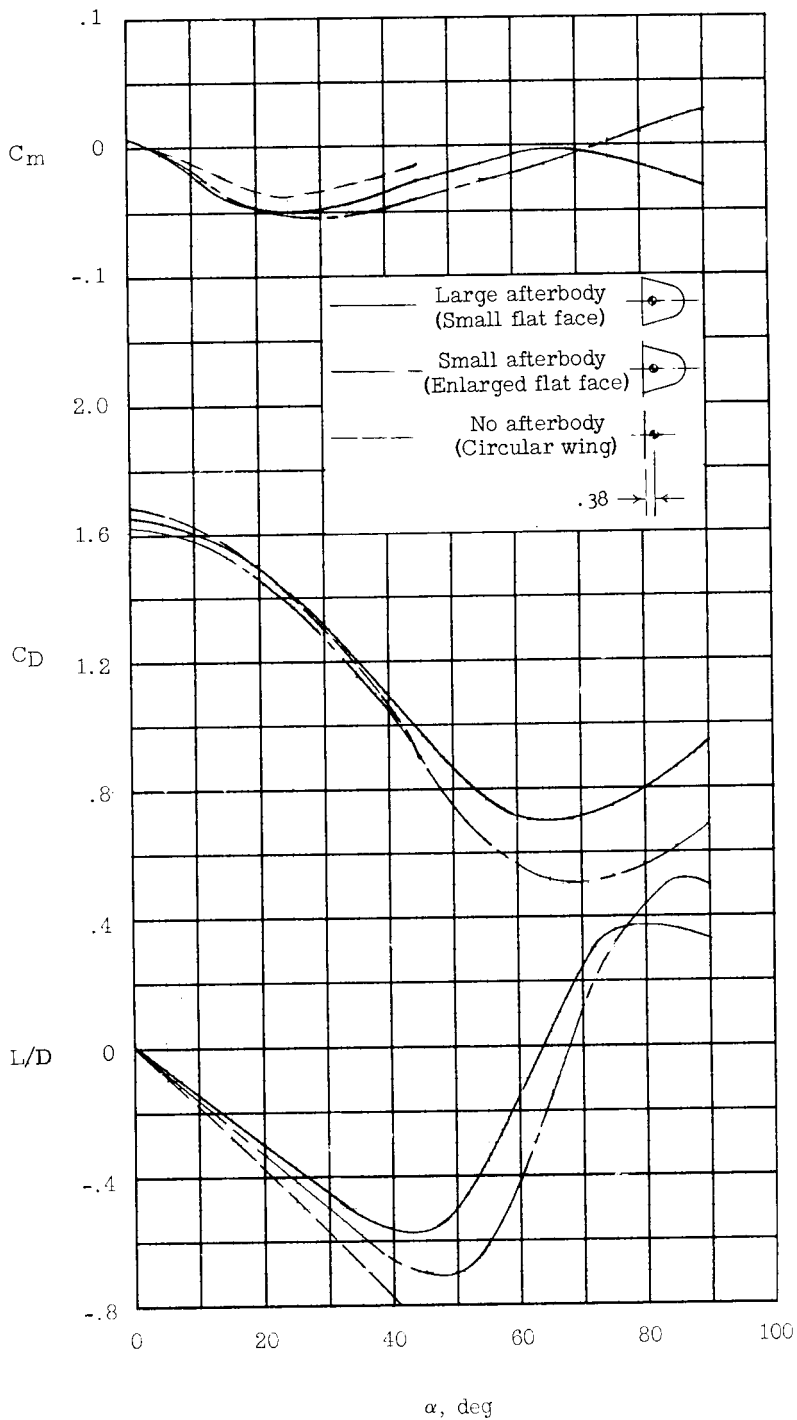
Figure 10.- Comparison of longitudinal stability characteristics of a
   basic reentry body with different afterbody size. M = 6.8; S, area
   of front face excluding flap.

Figure 11.- Trimmed longitudinal stability characteristics of convex-faced reentry body with trim flap. No lateral flaps; M = 6.8; S, area of front face excluding flap.

(a) $i_f = -45°$.

(b) $i_f = -90°$.

(c) $i_f = -140°$.

No flaps $\quad\quad$ $i_f = -45^\circ$ $\quad\quad$ $i_f = -90^\circ$

Circular wing; $\alpha = 0^\circ$

No flaps $\quad$ $i_f = -45^\circ$ $\quad$ $i_f = -90^\circ$ $\quad$ $i_f = -140^\circ$

Convex-faced reentry body; $\alpha = 0^\circ$; no lateral flaps
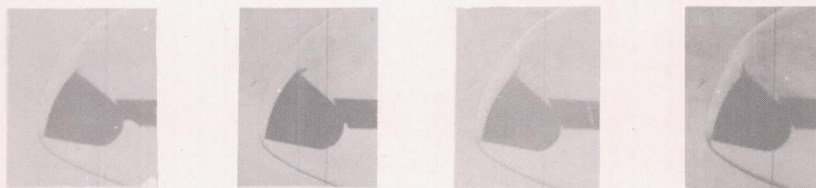
No flaps $\quad$ $i_f = -45^\circ$ $\quad$ $i_f = -90^\circ$ $\quad$ $i_f = -140^\circ$

Convex-faced reentry body; $\alpha = 25^\circ$; no lateral flaps

$\alpha = 0^\circ$ $\quad\quad$ $\alpha = -45^\circ$ $\quad\quad$ $\alpha = -90^\circ$

Convex-faced reentry body; $i_f = -90^\circ$; two lateral flaps

L-59-3070

Figure 12.- Schlieren photographs of the circular wing and convex-faced reentry body with and without flaps. M = 6.8.
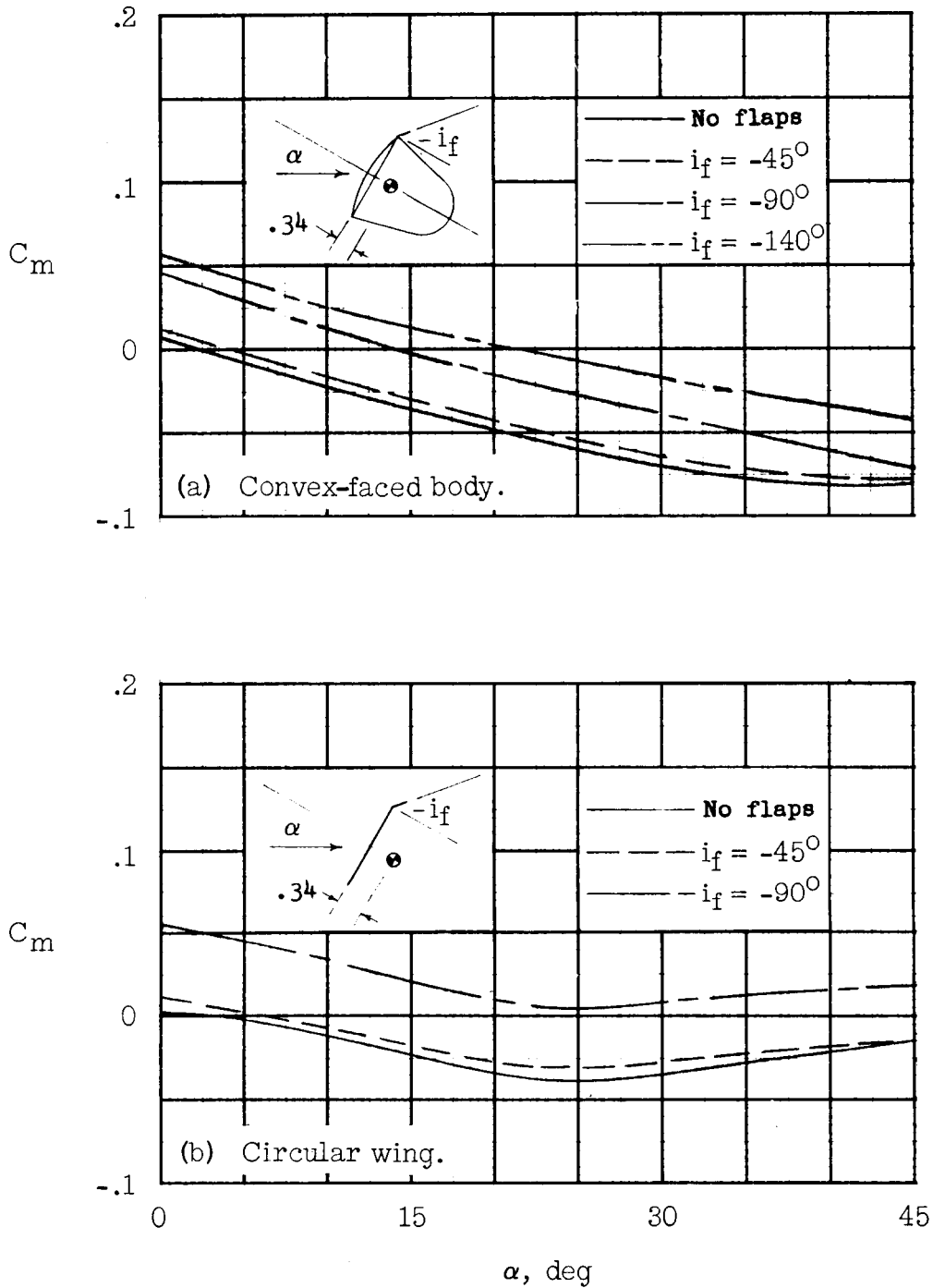
Figure 13.- Variation in the pitching-moment coefficient with different
flap deflections for the convex-faced reentry body and the circular-
wing plan form. M = 6.86; S, area of front face excluding flap.
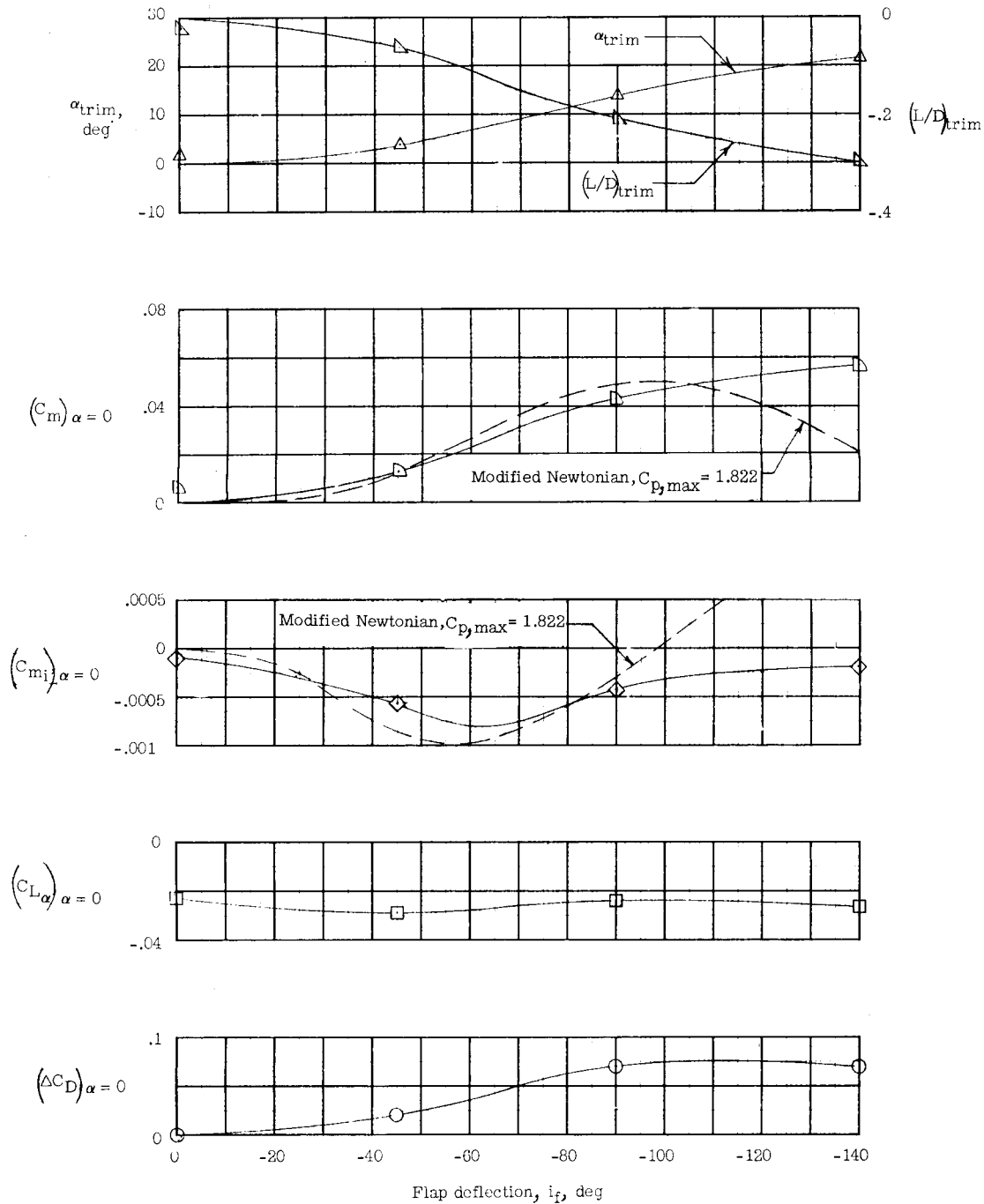
Figure 14.- Effect of trim flap deflection on the static longitudinal stability characteristics of the convex-faced reentry body. M = 6.8; from faired curves of basic data.
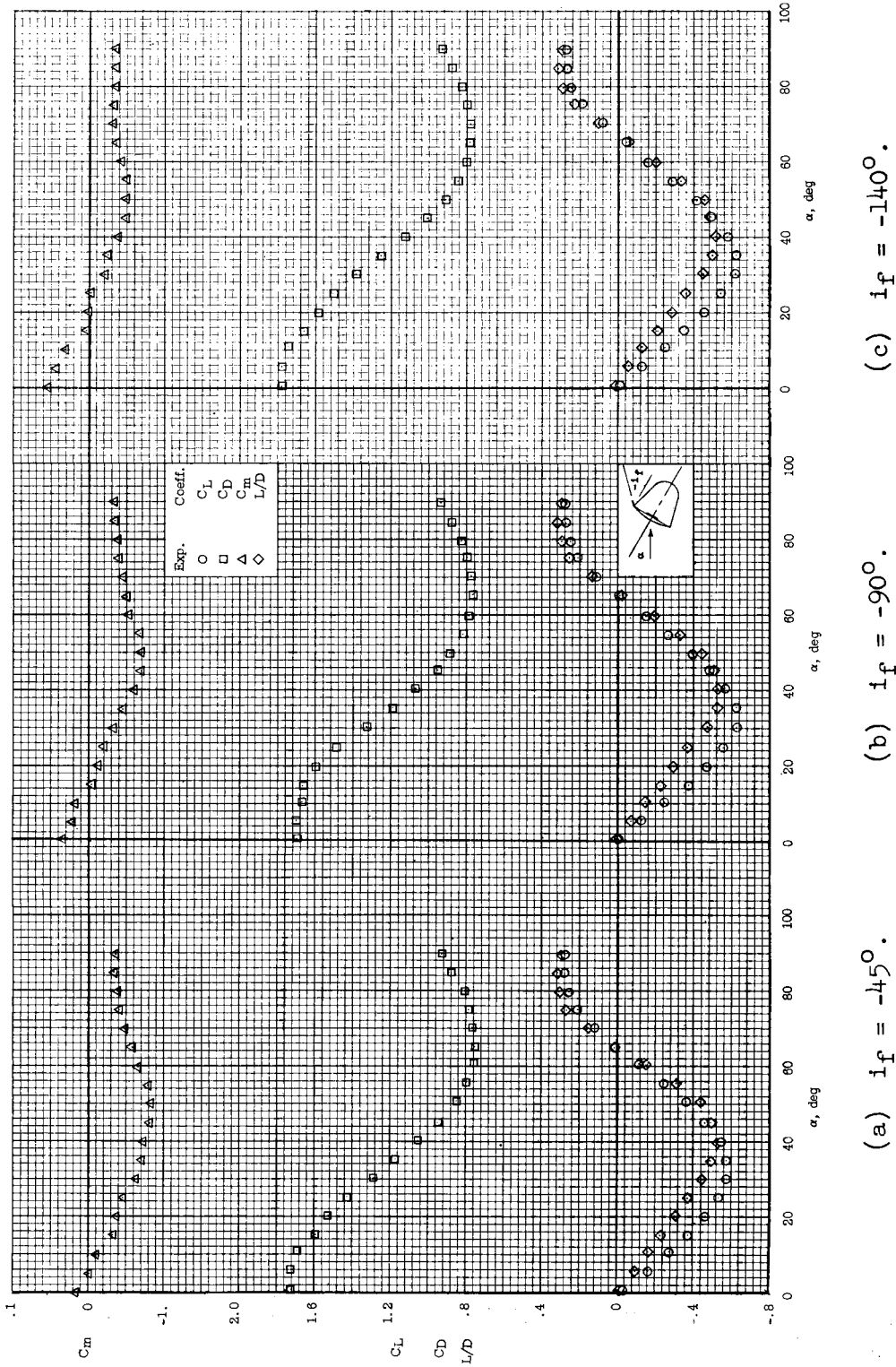
Figure 15.- Trimmed longitudinal stability characteristics of the convex-faced reentry body equipped with trim flap and two lateral flaps. M = 6.8; S, maximum body cross-sectional area.

(a) $i_f = -45^\circ$.   (b) $i_f = -90^\circ$.   (c) $i_f = -140^\circ$.
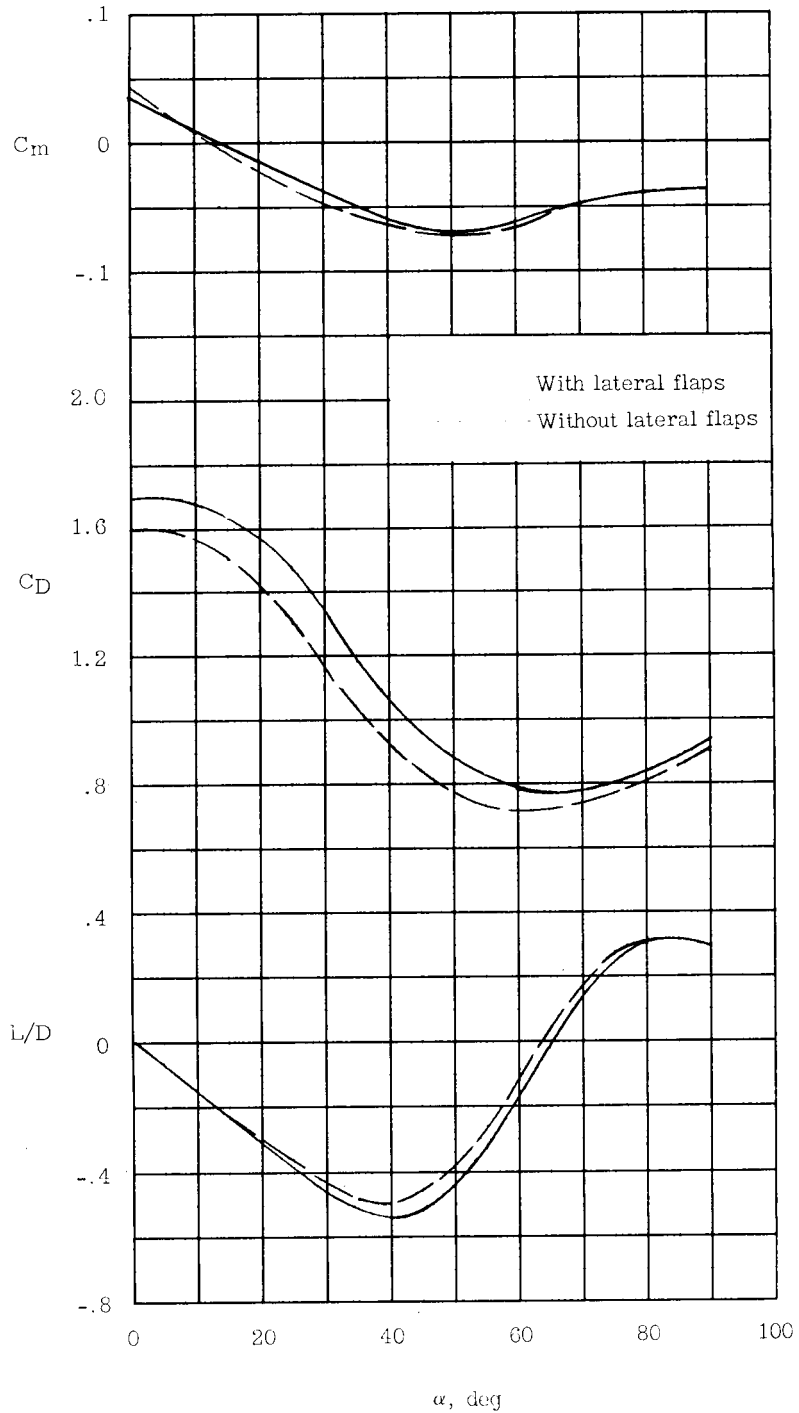
Figure 16.- Comparison of the longitudinal stability characteristics of the convex-faced reentry body with and without lateral flaps. $i_f = -90°$; $M = 6.8$.
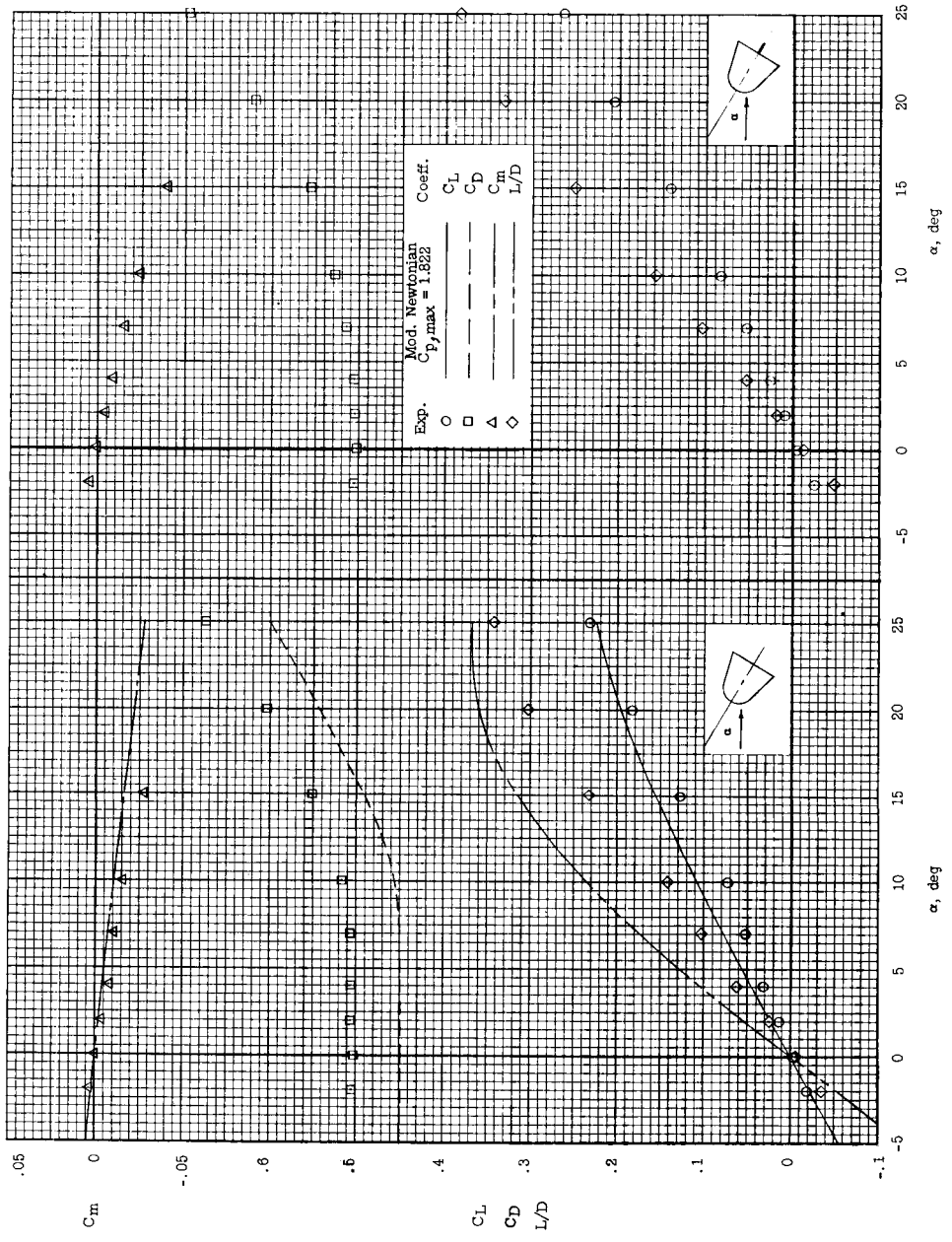
(a) No flaps.

(b) $i_f = 0^\circ$.

Figure 17.- Longitudinal stability characteristics of a blunt conical reentry body. M = 6.8; S, maximum body cross-sectional area.
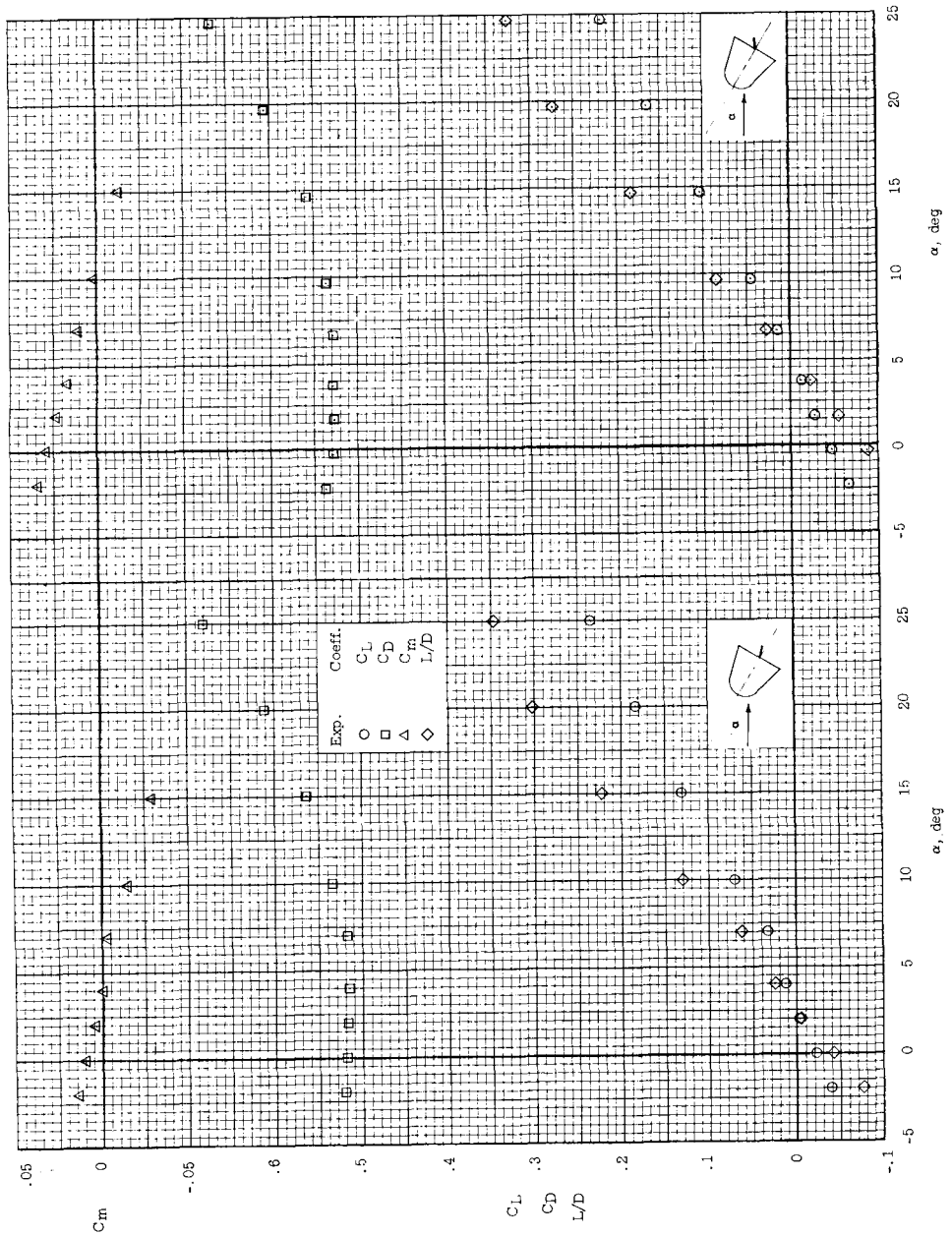
CONFIDENTIAL

(d) $i_f = -40°$.

(c) $i_f = -20°$.

Figure 17.- Concluded.

$\alpha = 0^{\circ}$
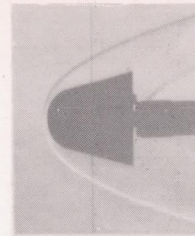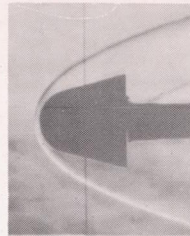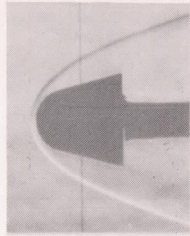
$\alpha = 15^{\circ}$

No flaps $i_f = 0^{\circ}$ $i_f = -20^{\circ}$ $i_f = -40^{\circ}$

L-59-3071

Figure 18.- Typical schlieren photographs of the blunt conical-nosed reentry body. M = 6.8.
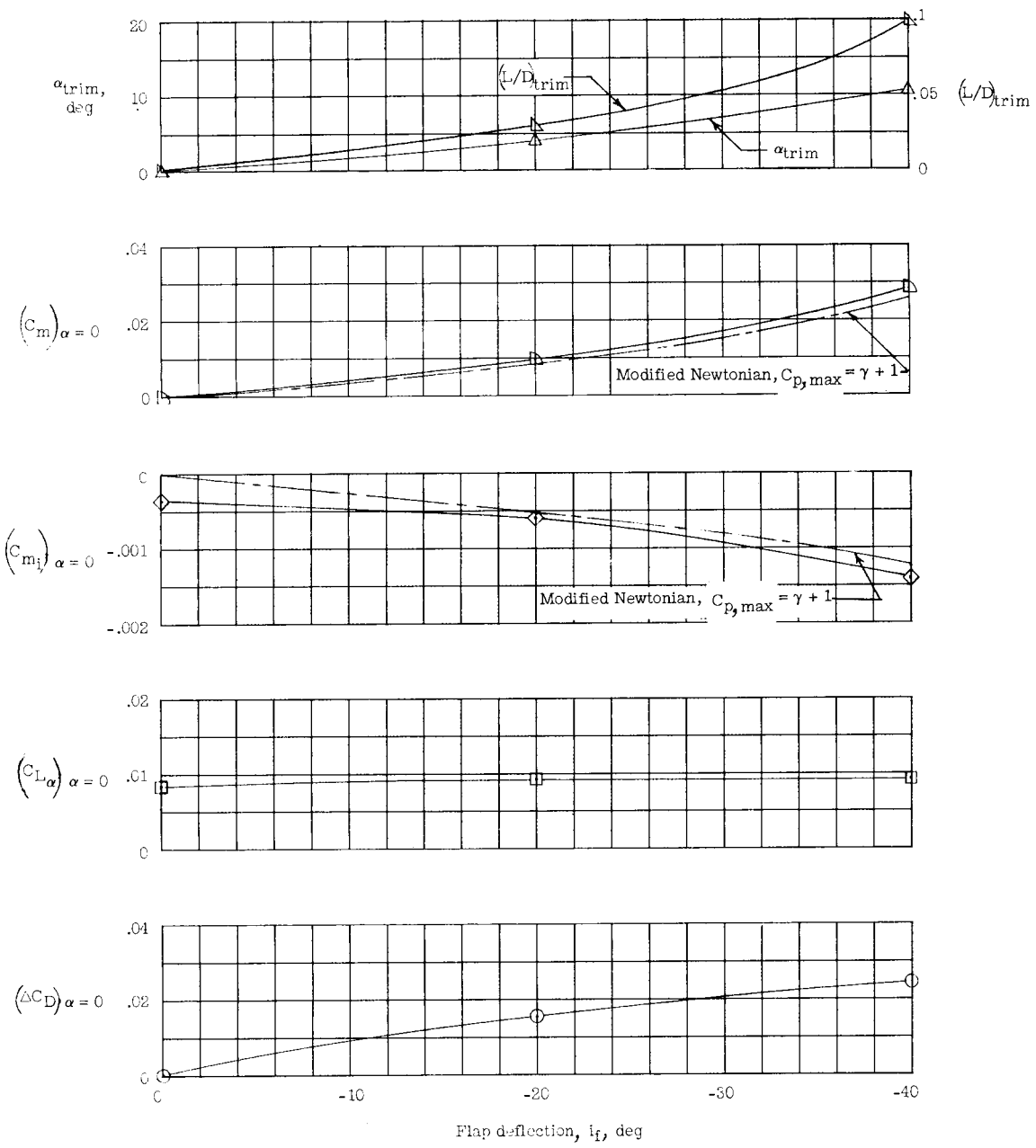
Figure 19.- Effect of flap deflection on the static longitudinal stability characteristics of the blunt conical reentry body. M = 6.8.